Separation Science and Technology
Publication details, including instructions for authors and subscription information:
http://www.informaworld.com/smpp/title~content=t713708471

Continuous Separation of Sugarcane Molasses with a Simulated Moving-Bed Adsorber. Adsorption Equilibria, Kinetics, and Application

M. Saska[a]; Mei Di Wu[a]; S. J. Clarke[a]; K. Iqbal[a]
[a] AUDUBON SUGAR INSTITUTE/SUGAR STATION LOUISIANA STATE UNIVERSITY AGRICULTURAL CENTER, BATON ROUGE, LOUISIANA

To cite this Article Saska, M. , Wu, Mei Di , Clarke, S. J. and Iqbal, K.(1992) 'Continuous Separation of Sugarcane Molasses with a Simulated Moving-Bed Adsorber. Adsorption Equilibria, Kinetics, and Application', Separation Science and Technology, 27: 13, 1711 — 1732
To link to this Article: DOI: 10.1080/01496399208019442
URL: http://dx.doi.org/10.1080/01496399208019442

SEPARATION SCIENCE AND TECHNOLOGY, 27(13), pp. 1711–1732, 1992

Continuous Separation of Sugarcane Molasses with a Simulated Moving-Bed Adsorber. Adsorption Equilibria, Kinetics, and Application

M. SASKA, MEI DI WU, S. J. CLARKE, and K. IQBAL
AUDUBON SUGAR INSTITUTE/SUGAR STATION
LOUISIANA STATE UNIVERSITY AGRICULTURAL CENTER
BATON ROUGE, LOUISIANA 70803

Abstract

Fundamental chromatographic properties are reported that are related to the industrial separation of sugarcane molasses in a simulated moving-bed adsorber. The distribution coefficients of KCl, sucrose, glucose, and fructose on XUS-40166.00 (K^+) cation exchanger were determined by pulse testing to be 0.00, 0.22, 0.45, and 0.50 at infinite dilution at 70°C. The adsorption isotherm of KCl is quadratic; those of the sugars only slightly nonlinear and dependent on KCl concentration. HETP was found to be independent of fluid velocity for KCl in the range of the interstitial velocity of 5 to 35 cm/min, and increasing with v for sucrose. At high fluid velocities the broadening of the sucrose band in a packed bed comes primarily from intraparticle mass transfer, with axial dispersion and film diffusion playing minor roles. The process for separation of sugarcane molasses was demonstrated on a 47-L, eight-column simulated moving-bed adsorber. A theoretical, staged model of the simulated moving-bed adsorber with one inert totally excluded and three linearly adsorbing components was found to give an excellent representation of the transient and steady-state behavior of the continuous separation of sugarcane molasses.

INTRODUCTION

The separation of sugars from nonsugars of sugarbeet molasses has gained commercial importance with the introduction to the sugar industry of the continuous simulated moving-bed (SMB) technology. The currently used SMB systems are all derived from the original UOP Sorbex process (*1*) except that the rotating distribution valve has in some cases been substituted with multiple solenoid valves to direct the flows into and out of the appropriate columns. Periodic switching of the inlet and outlet ports (Fig. 1) by one column in the direction of the liquid flow approximates the movement of the resin bed against the direction of the liquid flow.

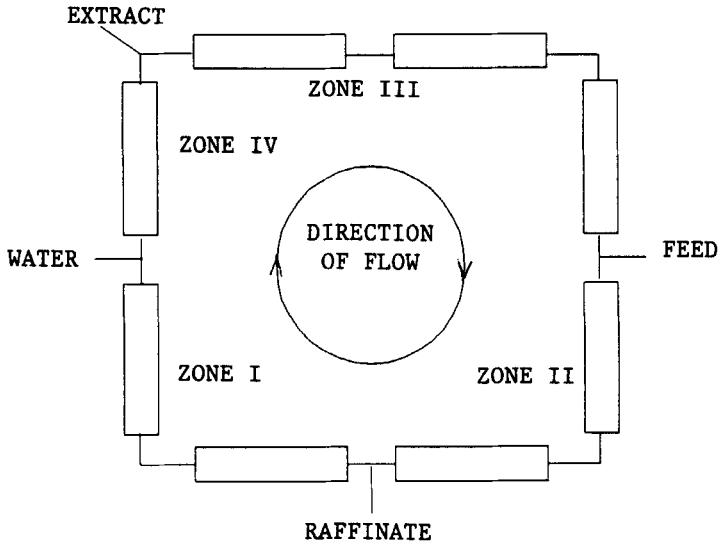

FIG. 1. Schematic of a 8-column SMB separator. The countercurrent operation is approximated by periodic switching of the inlet and outlet ports of one column along the direction of liquid flow.

Most frequently, the system is subdivided by the position of the ports into four zones of one or more columns each: zone I, where the fresh resin contacts the solution enriched with the fast component, resulting in a nearly solute-free liquid at the zone outlet to be recirculated into zone IV; zones II and III where the feed is fractionated into its components; and zone IV where the adsorbent is washed off the strongly retained (slow) components and conditioned for recirculation into zone I. The design then consists of choosing such flow rates and switch times that the net flows of the components are toward the appropriate ports and the desired purity of the products is achieved. A third outlet port may be added if a third fraction is desired with an intermediate mobility between the extract and raffinate components. The process has now been established as an economically viable one for increasing sugar recovery and production (*2–4*) in those areas of the world with conducive regulatory and pricing policies.

In recent work (*5*) we discussed the fructose/glucose equilibria on DOWEX Monosphere 99 CA resin and their application for design of an SMB process. It was found that contrary to some previous reports on similar adsorbents, the isotherms at industrial concentrations were nonlinear and coupled. The adsorption was anti-Langmuir, i.e., the differential adsorbed amount increased with the liquid concentration. Such behavior has been

observed in the adsorption of sugars and polysaccharides on porous adsorbents (*6–8*), and it is likely related to the progressive dehydration of the solute and adsorbent surfaces at increasing sugar concentrations (lower water concentrations) and strong adsorbate–adsorbate interactions.

Contrary to the glucose/fructose separation (Ca^{2+} form of the resin), almost no information is available in the open literature on the fundamental separation characteristics of the appropriate resins (strong cation exchangers in K^+ or Na^+ form) for the principal components that form the beet or cane molasses, e.g., sucrose, glucose, fructose, salts, colorants, polysaccharides, etc. Such characteristics in conjunction with the existing models of the SMB process (*5*, *8–10*) are required for an optimum design of an SMB adsorber. In this communication we give our results with adsorption of sucrose, glucose, fructose, and KCl on a Dow's XUS-40166.00 resin (K^+ form), a cation exchanger that has been in commercial use in the United States sugarbeet industry since 1988. Further, the effect on the separation efficiency of such important design parameters as loading of the resin (related to the throughput in industrial operation), temperature of the columns, and liquid flow rate are investigated. Moreover, experiments on our pilot eight-column simulated moving-bed adsorber are described and used to validate the dynamic model of the adsorber.

PROCEDURES

The columns were packed with fresh XUS-40166.00 cation exchanger (Dow Chemical Co., Midland, Michigan, lot MM 890421-1) in K^+ form. This polystyrene-divinylbenzene resin with 6% crosslinkage and a volume-based median pore size of around 10 Å has an ion-exchange capacity of about 2.0 meq/mL bed volume and a volume-based median particle diameter d_p of 390 μm (½ of the resin volume consisting of particles less than 390 μm, ½ of the volume of particles more than 390 μm). The extremely narrow size distribution of the resin particles minimizes the pressure drop on the columns and broadening of the components bands.

The adsorption isotherms were obtained from pulse testing that was done on two or four in-series jacketed glass columns of a nominal size of 210 × 6 cm i.d. (column volume 5940 mL) that are a part of our eight-column continuous adsorber. A predetermined mass (from 100 to 800 ± 1 g) of the feed solution was pumped slowly to the top of the first column and then eluted with deionized water at 150 mL/min (v = 13.6 cm/min). The pumps used were of an eccentric screw type designed such as to deliver a constant flow rate independent of the backpressure. The direction of the flow was downward in all columns so that the potential problems with fluidizing the resin bed at high flow rates and sugar concentrations were

minimized and the flow rate was frequently determined off-line (±0.1 mL/min) by measuring the time to collect the effluent in a precision volumetric flask. The temperatures of the elution and jacket waters were controlled to about ±2°C. The effluent from the columns was monitored with on-line preparative RI (Waters 404) and absorbance (Waters 440) detectors or at higher concentrations, where the response of the on-line RI detector was not sufficiently linear, with an off-line refractometer. The measured RI signals were converted to mass and volume concentrations using the standard tables (*11*) of solution properties. In the case of molasses, where the nonsugar fraction is a complex mixture, the RI signal was converted to concentrations assuming the RI vs c function of KCl, a prevalent component of the nonsugars. In the case of multicomponent feeds an HPLC with a carbohydrate column (Bio-Rad Aminex HPX-87K) was used. The effects of the flow rate on the chromatographic behavior of KCl and sucrose were determined with the same system while changing the interstitial velocity (flow rate) between 5 and 35 cm/min.

The pulse response signal was numerically integrated to give the mean and standard deviation (t' and σ) of the elution peaks:

$$t' = \int ctdt \Big/ \int cdt$$

$$\sigma^2 = \frac{\int c(t - t')^2 dt}{\int cdt}$$

The time t was measured from the moment of turning the elution water pump on. Therefore, the feed mass-weighted path length and bed volume for the feed to travel through differ slightly depending on the volume of the feed injected and were corrected assuming rectangular injection with the feed prior to eluting forming a plug $m_f/(\rho\epsilon A)$ long. The error introduced with this assumption is insignificant for the conclusions reached here.

Because of the thermal expansion of the resin, the system void volume ϵ varied somewhat with the temperature and was found to be on average 0.40, 0.39, and 0.38 at 30, 50, and 70°C, respectively, from pulse tests with a high molecular weight dextran.

The effect of the ionic composition of the resin on sucrose/nonsugars separation was evaluated with pulse testing on a 100 × 2.5 cm i.d. LCD/Milton-Roy Cheminert chromatography column connected to the two on-line detectors. Prior to packing the column, the resin was equilibrated off-column with an excess of filtered sugarcane molasses (30% w/w) of various

Ca^{2+}/Mg^{2+} contents. The ionic composition of the resin was determined by stripping 25 mL of the resin packed in a standard 1 cm i.d. burette with a strong HCl, and titrating an aliquot of the properly diluted extract with EDTA for Ca^{2+}/Mg^{2+} determination and by flame photometry for K^+.

Derivation of the Adsorption Isotherms

The coefficients K_{0i}, A_i, and B_i of the quadratic binary isotherms (i = component 1, j = component 2)

$$K_i \equiv q_i/c_i = K_{0i} + A_i c_i + B_i c_j$$

were obtained by graphically matching the experimental pulse response signals, all measured at an identical flow velocity, v = 13.6 cm/min, with those calculated from a local equilibrium model

$$\partial c/\partial t + [(1 - \epsilon)/\epsilon]\partial q/\partial t + v(\partial c/\partial z) = 0$$

K_{0i}'s were obtained from pulse testing with single component feeds at infinite dilution ($A_i = B_i = 0$; $i = 1, 2$), while A_i's were obtained from testing with single component feeds of varied concentrations ($B_i = 0$; $i = 1, 2$) and with K_{0i}'s fixed from infinite dilution tests. The cross-coefficients B_i were determined for 1:3 KCl/sucrose binary feeds only. In the above equation, the time and space partial derivatives were replaced as usual with finite differences of the forward and backward types respectively (*10*) and solved on a 386-based PC. The nonlinearities from the form of the distribution coefficients were accommodated with an internal iteration procedure. The time and length integration steps of the discretized equation were chosen such as to match the profiles of low concentration pulse responses as in our previous work on glucose/fructose mixtures (Fig. 1 of Ref. *5*) and thus substitute for the lack of explicit axial dispersion terms (axial mixing and mass transfer) in the master equation.

The use of a local equilibrium model in a finite difference integration scheme does not imply that mass transfer does not play a role in determining the chromatographic behavior, which indeed is found to be the case here for sucrose at lower temperatures. Rather, the mass transfer and other dispersive effects are included in a semiempirical way (*12*) through a judicious choice of the time and space integration steps (Fig. 2).

Our reasons for using a numerical solution of the simplified equation for column behavior in modeling the pulse testing are that, first, the necessary condition in analytical solutions of linear adsorption is frequently unacceptable on porous nonrigid adsorbents, particularly in the case of

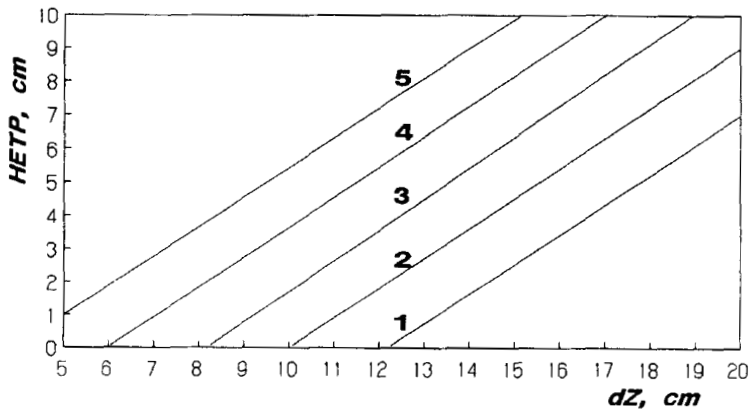

FIG. 2. Simulated chromatographic HETP at various flow velocities and integration length steps. Interstitial velocity (v, cm/min): 1, 51; 2, 43; 3, 34; 4, 26; 5, 17. L = 150 cm, dT = 0.3 min.

ionic species in ion-exclusion applications. Second, inclusion of explicit terms in the above master equation that would account for solid phase and liquid film transports and axial diffusion, although feasible, would preclude a fast numerical solution on a personal computer of the dynamic behavior of the simulated moving-bed adsorber. Hopefully, this will find practical use in designing and optimizing future simulated moving-bed applications.

The Simulated Moving-Bed Adsorber

Designed and built by Applexion S.A., a supplier of chromatographic and ion-exchange systems in Epone, France, the separator consists of eight glass jacketed 210 × 6 cm i.d. columns kept at ~70°C with a temperature-controlled hot water source. Each of the columns is associated with six solenoid valves controlled with a standard commercial process control software (LABTECH Control). Periodic switching of the valves at constant intervals advances the location of the inlet and outlet ports and simulates the countercurrent motion of the adsorber bed against the liquid flow (Fig. 1). Four precision eccentric screw pumps measure the flow of feed, water, extract, and recycle. The pressure within the system is controlled with a valve on the raffinate outlet. The flow in all columns is downward to avoid problems with fluidizing the packed bed at higher flow rates. The system was operated with one column in the resin regeneration zone (IV), three columns in the extract zone (III), two columns in the raffinate zone (II), and two columns in the recycle zone (I).

Modeling the Simulated Moving-Bed Adsorber

As in modeling the pulse tests, the algorithm based on the discretized local equilibrium PDE was used in the SMB modeling, now, of course, with the time-dependent boundary conditions (concentrations at the column inlets) and the discontinuities of the boundary conditions at times when the ports are switched along the direction of the flow. Because the flow rates and HETP characteristics in the columns may vary significantly between zones depending on the design, we allow for zone-dependent dZ, the integration length of the master equation, by matching the concentration profile of a column crossing the zone boundary such as to preserve the total solute mass within the column. dZ's are again chosen based on the HETP characteristics from pulse testing (Fig. 9) and pulse simulation (Fig. 2) at a given flow rate.

RESULTS AND DISCUSSION

Effect of Column Loading

The adsorption of all components studied and that of KCl in particular are concentration dependent. While the sugar elution profiles are nearly Gaussian (Fig. 3), with increasing concentration the KCl peaks become nearly triangular with a slowly increasing front and a steep tail (Fig. 4). This, of course, is because the rate of migration of the solute (KCl in this case), proportional to $\delta c/\delta q$, is faster at low concentrations. Then, as the band travels through the column, the front or downstream part of the band and the tail or upstream part of the band travel slower compared to the high concentration center.

The retention time t' and volume V' ($= Ft'/AL'$) generally increase with the column loading (Fig. 5) although the effects for the three sugars are relatively minor and linear within the range of experimental errors. The retention volume V' of KCl increases rapidly from around 0.39 ($\approx \epsilon$) at infinite dilution up to 0.58 at loadings of 12 g KCl per liter bed volume. This maximum loading corresponds to curve 7 in Fig. 4 or 803 g of 15.4% KCl solution fed. Despite the fact that the mass-averaged retention time t' of KCl becomes larger than that of sucrose above loadings of around 8 g/L, the separation is still possible (Fig. 6) although the recovery, i.e., the percent mass of sucrose in the sucrose-rich product, is reduced drastically at higher salt loadings. The curve S in Fig. 6 assumes no interaction between KCl and sucrose as it was calculated from numerical integration of the overlaid elution profiles of KCl (single component feeds) at various loadings with that for sucrose at a loading of 65 g/L. On the other hand, B was calculated from profiles obtained by feeding 1:3 KCl:sucrose solutions of varying total concentrations.

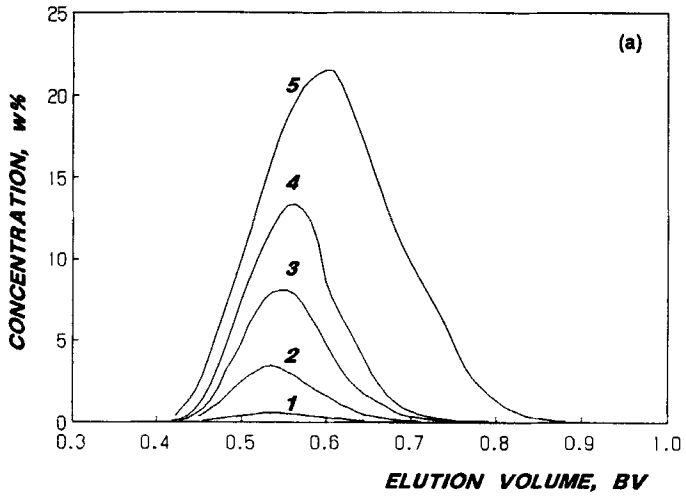

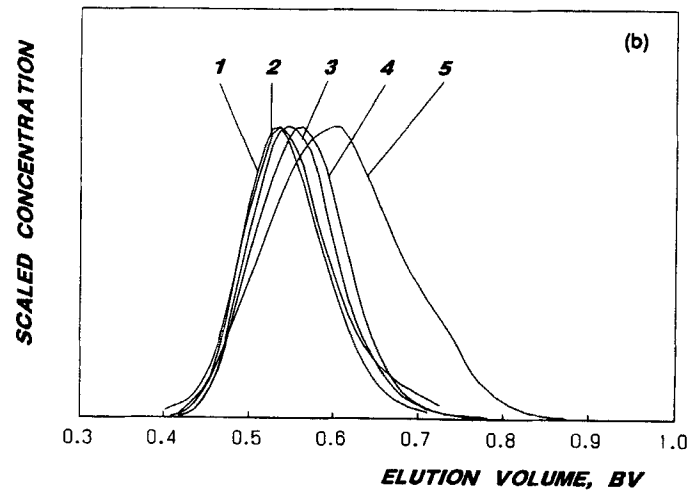

FIG. 3. Measured (a) and scaled (b) elution profiles of sucrose solutions at 70°C and 150 mL/min (v = 13.6 cm/min) at various column loadings: 1 = feed mass m_f 359 g, feed concentration 2.1%; 2 = 364 g, 11.6%; 3 = 279 g, 36.6%; 4 = 303 g, 61.1%; 5 = 766 g, 61.1%. The elution volume was calculated as Ft/AL', where the effective column length $L' = L - \frac{1}{2}L_f = L - \frac{1}{2}m_f/(\rho\epsilon A)$.

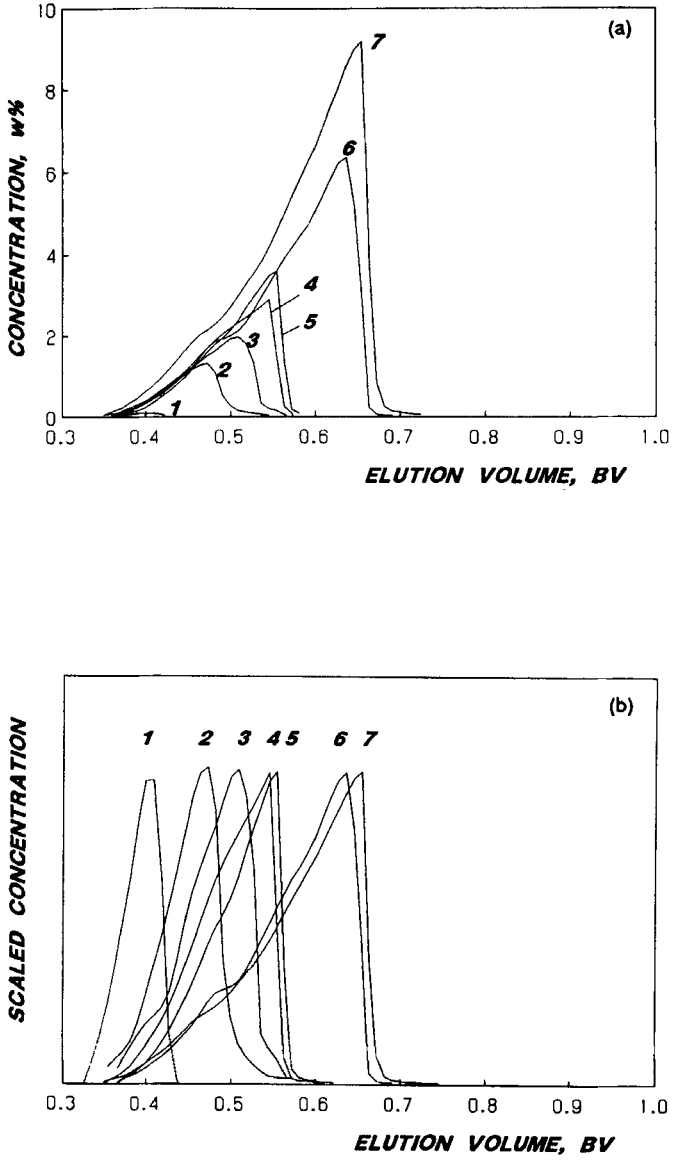

FIG. 4. Measured (a) and scaled (b) elution profiles of KCl solutions at 70°C and 150 mL/min (v = 13.6 cm/min) at various column loadings: 1 = feed mass m_f 246 g, feed concentration 0.5%; 2 = 378 g, 2.4%; 3 = 753 g, 2.4%; 4 = 263 g, 10%; 5 = 268 g, 15.4%; 6 = 789 g, 10%; 7 = 803 g, 15.4%. The elution volume was calculated as Ft/AL', where the effective column length $L' = L - \frac{1}{2}L_f = L - \frac{1}{2}m_f/(\rho\epsilon A)$.

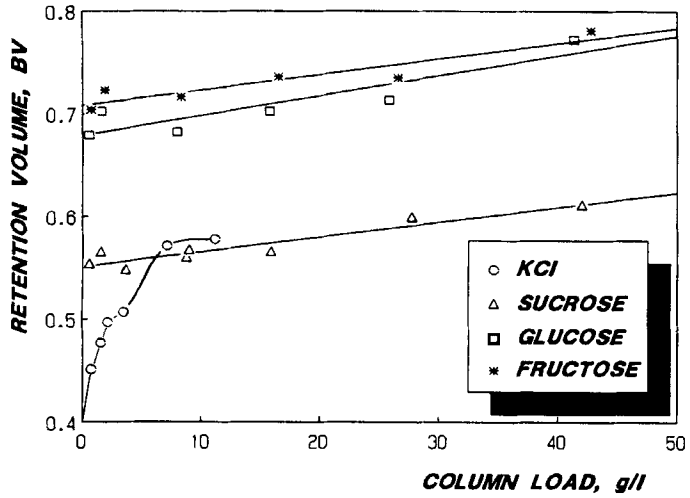

FIG. 5. Retention volumes V' ($= Ft'/AL'$) of KCl, sucrose, glucose, and fructose at 150 mL/min and 70°C at various column loadings. Both the feed volumes and concentrations were varied (see legends to Figs. 3 and 4). Single component feeds. The retention and effective bed volumes were corrected for the variable feed volumes as in Figs. 3 and 4.

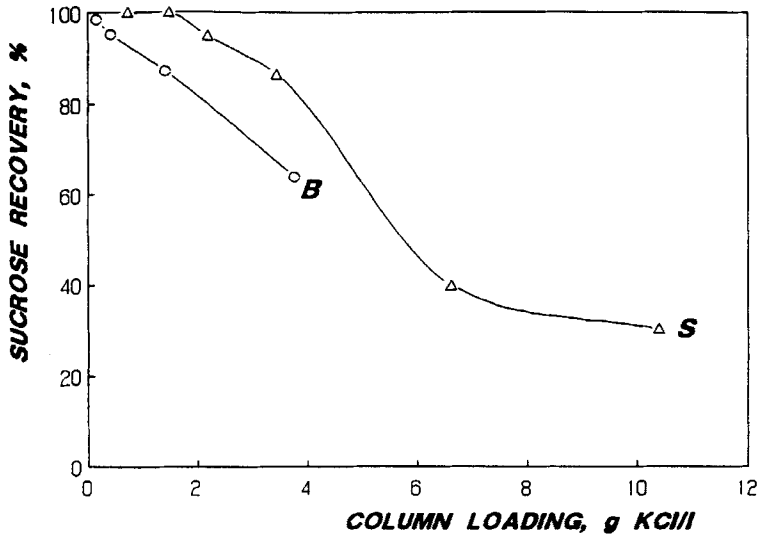

FIG. 6. Calculated recovery of sucrose in batch chromatography experiments in the sucrose-rich product of 95% purity at various loadings of the column expressed in g KCL per L resin bed. B = binary feeds, 1:3 KCl/sucrose. S = calculated from single component feeds elution profiles at a sucrose loading of 65 g sucrose per L resin bed. All runs at ~150 mL/min.

TABLE 1
Parameters of the Adsorption Isotherms Determined at 70°C on XUS-40166.00 Resin. The Numbers in the Parentheses are the Standard Deviation and Number of Experimental Points, Respectively. The Cross-Coefficients Were Determined Only for 1:3 Mixtures of KCl and Sucrose at Total Concentrations from 3 to 40% and Two Feed Volumes of 300 and 800 mL. $K_i \equiv q_i/c_i = K_{0i} + A_ic_i + B_ic_j$ (if i = sucrose, then j = KCl; if i = KCl, then j = sucrose).

i	T (°C)	K_{0i}	A_i	B_i
KCl	70	.000	0.64 (.016,6)	.026 (.038,12)
	50	.013	—	—
	30	.033	—	—
Sucrose	70	.215	.004 (.001,6)	.018 (.013,8)
	50	.223	—	—
	30	.235	—	—
Glucose	70	.450	.004 (.002,5)	—
Fructose	70	.495	.003 (.002,5)	—

The linear coefficients K_i of the adsorption isotherms (Table 1) are respectively 0.000, 0.215, 0.450, and 0.495 for KCl, sucrose, glucose, and fructose. As expected, KCl is totally excluded from the resin at infinite dilution but is retained considerably by the resin at higher concentrations as indicated by the large quadratic term. It is interesting to note that the sucrose/invert separation (invert = a glucose/fructose mixture) on the K^+ resin is nearly equivalent to the separation of glucose/fructose on the Ca^{2+} form of the same resin (*5*) with K_0 of 0.245 and 0.47, respectively. The curvatures of the isotherms of the three sugars are small and nearly identical, with the average value of 0.004 comparable to the self- and cross-coefficient found for glucose and fructose on a Ca^{2+} resin in our previous work. This indicates that the mechanisms leading to the nonlinearities of the respective isotherms may be similar for the sugars involved and fairly independent of the ionic form of the resin. The uncertainty in the cross-coefficients, though, for the KCl/sucrose mixtures is large. The shrinkage of XUS-40166.00 (K^+) in sugar and salt solutions is comparable to that of DOWEX Monosphere 99 CA (Ca^{2+}) resin (*5*), and this may contribute further to the nonlinearities observed in both cases.

As in the case of glucose/fructose mixtures, the mutual positive (adsorption enhancing) interaction of KCl and sucrose slows down the front of the slower component, i.e., sucrose (Fig. 7), and makes the peak narrower and taller than it would be if no interaction occurred. This, though, is in apparent contradiction to the batch adsorption experiments on DOWEX 50W X4 (K^+) of Meyer (*13*) who found at 90°C a reduction in sucrose adsorption on increasing the solution concentration of KCl. In the

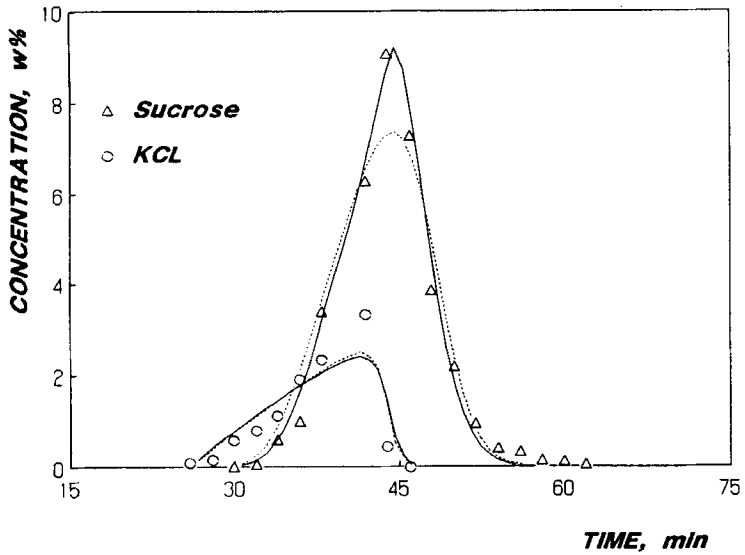

FIG. 7. Elution profiles of 1:3 KCl:sucrose mixture (circles and triangles are the experimental points), 791 g solution fed of a total concentration of 25%. Two columns in series, flow rate 150 mL/min, 70°C. The lines are theoretical models with the following isotherms. Dashed line: "Best" nonlinear uncoupled isotherms, $K_{KCl} = 0.067c^2$, $K_{sucrose} = 0.235c + 0.0085c^2$. Solid line: "Best" nonlinear coupled isotherms, $K_{KCl} = 0.064c^2 + 0.0015c_ic_j$, $c_{sucrose} = 0.235c + 0.003c^2 + 0.02c_ic_j$ (i = sucrose, j = KCl).

same work the adsorption isotherm of KCl was found to be quadratic and the amount of KCl adsorbed increased with increasing liquid concentrations of sucrose, similar to what was found in this work.

Effect of Flow Rate and Temperature

Subject to the pressure drop constraints, the flow rate within the columns is one of the parameters in an SMB operation that can be varied within certain limits and used for optimizing the separation. It is therefore important to know how the behavior of the major components is affected by the flow rate and to what extent it deviates from the equilibrium conditions. In particular, the widening of the component bands, expressed as the (dimensionless) standard deviation σ/t' of the peak or the height equivalent to a theoretical plate (HETP) $[= L'(\sigma/t')^2]$ are frequently observed to increase with increasing flow rate and adversely affect the separation.

The retention times and bandwidths were determined (Fig. 8) for KCl and sucrose at infinite dilution at three temperatures, 30, 50, and 70°C, at

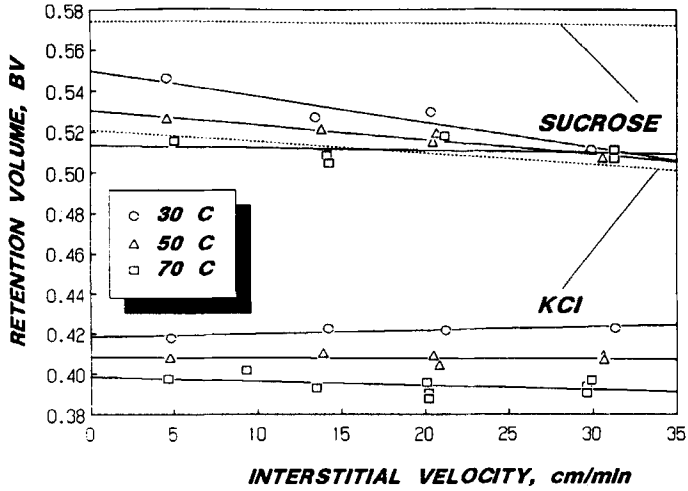

FIG. 8. Effect of the flow rate and temperature on the retention volume V' of sucrose and KCl (single component feeds) at infinite dilution (300 g of 0.5% solution fed in each case). Symbols and solid lines: Experimental points and their least-squares fits. Dotted lines: Retention volumes V' of sucrose (upper line) and KCl (lower line) at high concentrations and 70°C (300 g of 61 and 15% solutions of sucrose and KCl fed, respectively).

flow rates from 50 to 350 mL/min (interstitial velocity from 5 to 32 cm/min). In addition, for sucrose the behavior was also measured at a higher concentration at 70°C, conditions more representative of the industrial SMB operation. While V', the retention volume of KCl, is practically independent of the flow velocity, for sucrose it decreases at higher flow rates and more so the lower the temperature. As will be discussed more thoroughly in the following, the process that dominates the rate of adsorption of sucrose is the rate of diffusion of the molecules inside the resin particles. At higher liquid flow rates the sucrose molecules within a band moving past an element of the resin do not have enough time to penetrate all the internal pores that they would under equilibrium conditions. Then the band as a whole travels through the column faster relative to a nonretained species ($V' = \epsilon$) than it would at lower liquid velocities. As the diffusion coefficient of sucrose becomes smaller at lower temperatures, this behavior becomes more pronounced. At and above 70°C, i.e., conditions in the existing industrial, simulated moving-bed adsorbers in the sugarbeet industry, even at higher concentrations and up to $v = 35$ cm/min, the kinetics of liquid–solid mass transfer is faster than the rate of band movement down the column, and the local equilibrium prevails.

HETP, the height equivalent to a theoretical plate, is nearly independent of v for KCl (at infinite dilution); peak broadening is from eddy diffusion only and a linear function of v at higher temperatures for sucrose (Fig. 9). The intercept at $v = 0$ ($= 2D_L/v$) of all lines is nearly identical for both KCl and sucrose regardless of the temperatures, giving an axial dispersion coefficient (cm^2/min) of

$$D_L \approx 0.3v$$

or about 15 times less than found by Ching and Ruthven (*14*) for glucose and fructose on 300 μm (d_p) Duolite C-204 and 5 times less than found in our previous work (also glucose and fructose on 320 μm Dowex Monosphere 99 CA) but rather close to $0.2v$ determined by Goto (*15*) for NaCl and sucrose on a 326-μm ion-retardation resin. The limited data at higher sucrose concentrations (the dotted line in Fig. 9) indicate that the dispersion coefficient becomes larger

$$D_L \approx v$$

perhaps because of the gravity effects on peak dispersion in the vertical columns. The overall mass transfer coefficient k defined as

$$\delta q/\delta t = k(Kc - q)$$

of sucrose was calculated from the slopes at $v = 0$ of the HETP vs v curves (*14*)

$$\delta(\text{HETP})/\delta v = 2f(1/Kk)(1 + f/K)^{-2}$$

$$f = \epsilon/(1 - \epsilon)$$

to be 0.73, 1.7, and 2.2 min^{-1} at 30, 50, and 70°c, respectively (Table 2), and independent of the fluid velocity at and above 50°C. At 30°C, the slope of the HETP vs v curve becomes smaller and the overall mass transfer coefficient larger at higher flow rates and nearly equal to those at 50 and 70°C. This indicates the film mass transfer to be important at low temperatures and low fluid velocities, although k would still be expected at high fluid velocities to be lower at lower temperatures because of the likely temperature effect on the intraparticle diffusivity. As the slope of the HETP vs v line (proportional to $1/Kk$) is, at least at 70°C, independent of concentration, $k \approx 1/K$ and the overall mass transfer coefficient is expected to decrease slightly with an increase in sucrose concentration.

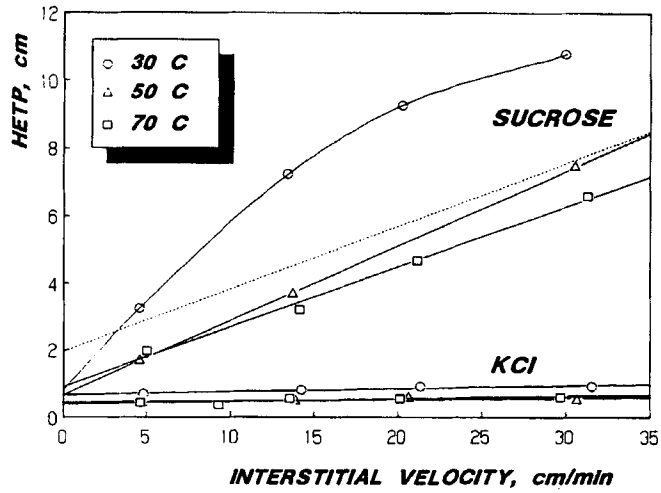

FIG. 9. Effect of the flow rate (or fluid velocity v) and temperature on the height equivalent to a theoretical plate (HETP). Single component feeds. Solid lines and symbols: Infinite dilution, i.e., 300 g of 0.5% solution fed in each case. Dotted line: HETP of sucrose at 70°C and a high concentration (300 g of a 61% solution fed). HETP was calculated as $L'(\sigma/t')^2$.

To further clarify the respective contributions of the axial dispersion and the mass transfer effects, be it in batch or continuous chromatography, to the overall HETP,

$$\text{HETP} = L'(\sigma/t')^2 = \text{HETP}_{\text{axial}} + \text{HETP}_{\text{film}} + \text{HETP}_{\text{intra}}$$

the empirical correlation of Wakao (*16*) was used to calculate the mass transfer coefficient for diffusion of sucrose through the film layer outside

TABLE 2

The Calculated Film Mass Transfer Coefficients k_f of Sucrose (*16*), and the Overall Mass Transfer Coefficients Determined Experimentally. Diffusion Coefficients of Sucrose of 3.5, 5.4, and 8.9 × 10^{-4} cm^2/min at 30, 50, and 70°C Were Used in the Calculation. The Specific Surface Area a of the Resin Is 154 cm^2/mL.

	v (cm/min)	30°C	50°C	70°C
k, min^{-1}	—	0.73	1.7	2.2
$k_f a$, min^{-1}	5.0	9.2	13.9	20.3
	20.0	15.7	23.1	34.2
	30.0	18.5	26.8	40.7

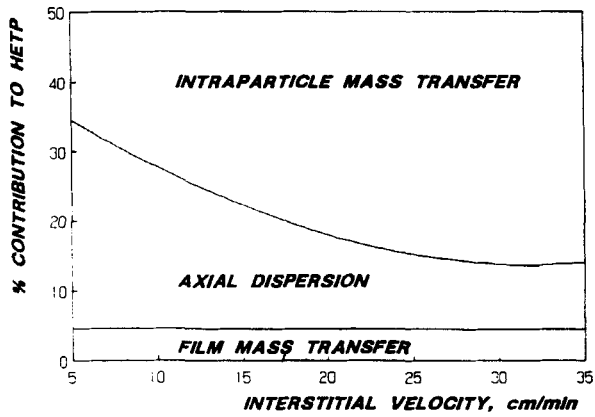

FIG. 10. Relative contributions of the three major band broadening factors to the overall HETP. Sucrose at infinite dilution and 70°C.

the resin particles (Table 2). HETP from the film transfer resistance was calculated as (*14*)

$$\mathrm{HETP}_{\mathrm{film}} = 2f(v/Kk_fa)(1 + f/K)^{-2}$$

where the overall mass transfer coefficient k in Eq. (5) of Ching and Ruthven (*14*) was replaced with k_fa. With $\mathrm{HETP}_{\mathrm{axial}} = 2D_L/v$ (*14*) and at infinite dilution, the individual contributions are only slightly dependent on temperature and are dominated, as expected, by intraparticle mass transfer that makes up (Fig. 10) 55% of HETP at $v \rightarrow 0$ and over 85% at high flow rates. The axial dispersion adds around 30 and 10% at low and high flow rates, respectively. The contribution of the film mass transfer is minor, about 5% and independent of the flow rate.

SMB Separation of Sugarcane Molasses

When appropriately pretreated sugarcane final molasses are passed through a column packed with the cation exchanger, they either completely or partially separate into their major components: nonsugars, sucrose, glucose, and fructose (Fig. 11). The nonsugar part of molasses that forms about 40% of dry matter is known to consist of many components, some of them as yet unidentified, that fall into several broad categories: inorganic and organic salts, native and bacterial polysaccharides, colorants with a range of chemical properties and molecular sizes, etc. Of the nonsugar components, the colorants, presumably on account of their high molecular

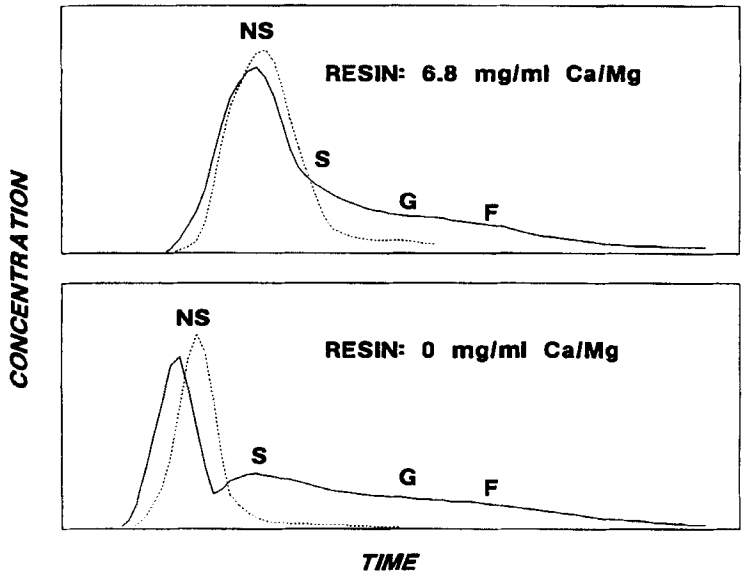

FIG. 11. Pulse tests on a column packed with fresh XUS-40166.0 resin (K^+, bottom) and the same resin with 6.8 mg/mL Ca^{2+}/Mg^{2+}. The total resin capacity is 2.0 meq/mL or 78.0 mg/mL K^+ for the fresh resin. Column 100 × 2.5 cm i.d., flow rate 4.5 mL/min. Two on-line detectors in series: RI (solid lines), absorbance at 436 nm (dotted lines). Feed: 3 mL of 33% (w/w) clarified, filtered molasses.

weight, travel through the column fastest with the exception of a small fraction of colorants that appear to adsorb on the resin and elute very slowly. Even small traces of calcium and magnesium on the resin, of the order of 0.1 meq/mL of the resin bed (out of the total capacity of 2.0 meq), cause a noticeable reduction of the separation efficiency (Fig. 11). Sucrose is progressively less retained by the resin as potassium is replaced with calcium on the resin (*6*). At the same time, the ionic species, nearly totally excluded from the resin at low concentrations on a K^+ resin, are more strongly retained on the Ca^{2+} form of the ion exchanger. Both these factors contribute to worsening of the separation of sucrose from nonsugars.

Precipitation of divalent ions with phosphoric acid followed by pH adjustment with alkali reduces the Ca^{2+}/Mg^{2+} content below 3,000 ppm (dry basis) from the initial 10,000 or so. The still relatively high Ca^{2+}/Mg^{2+} content can apparently be tolerated because of the relatively high content of the competing potassium, 5% of the total dissolved solids or more, of the Louisiana molasses that were used in our experiments.

The results of a 30-h experiment are shown in Figs. 12–14. With the system initially filled with water, the steady-state compositions are achieved after about 7 h or 6 full cycles. Extract, the sucrose-enriched product, consists on a dry basis on average of 82% sucrose, 15% invert (glucose + fructose), and 3% nonsugars. Raffinate contains 70% nonsugars, 22% invert, and 8% sucrose. The sucrose recovery is about 90%, and the overall product concentrations are 28% (w/w) and 6% for extract and raffinate, respectively, for a 60.5% feed.

A summary of two earlier experiments done at identical conditions with the exception of feed composition and concentration are listed in Table 3. Treatment of the molasses prior to SMB separation involved phosphatation with H_3PO_4 to a pH of 3.8, followed by raising the pH to 7.4 with NaOH, and filtration on a rotating membrane system. This reduced the concentration of the divalent ions to 2900 ppm from the initial 8700 ppm and produced an opticaly clear filtrate. While nonsugars and sucrose are concentrated, as expected, in the raffinate and extract, respectively, the invert (glucose and fructose) partitions approximately equally into the two products. Introduction of a third outlet port for invert is feasible and will depend on the economic analysis of the process. If liquid sweetener is to be produced, separation of sucrose from invert is not required. On the other

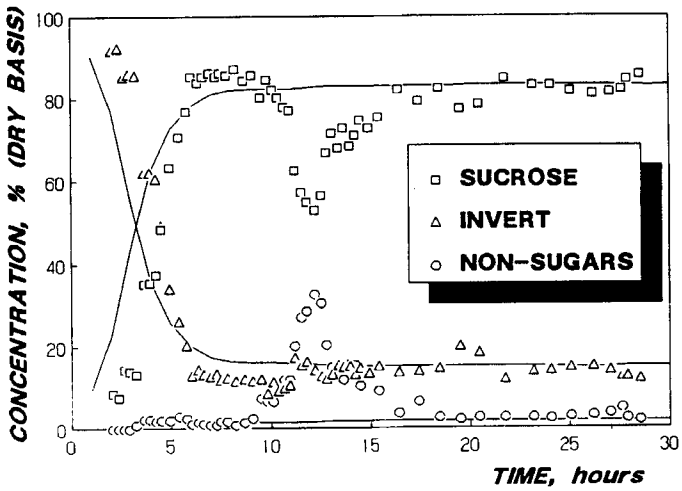

FIG. 12. Experimental (points) and simulated (lines) composition of the extract. Feed: 60.5% (w/w); sucrose (% dry basis), 50.0; invert, 21.1; nonsugars, 28.9. Flow rates (mL/min): feed, 20; water, 120; extract, 30; raffinate, 110; recycle, 280. Flow velocities in zones (v, cm/min): I, 24.2; II, 33.6; III, 31.9; IV, 34.5. Switch time: 8.6 min.

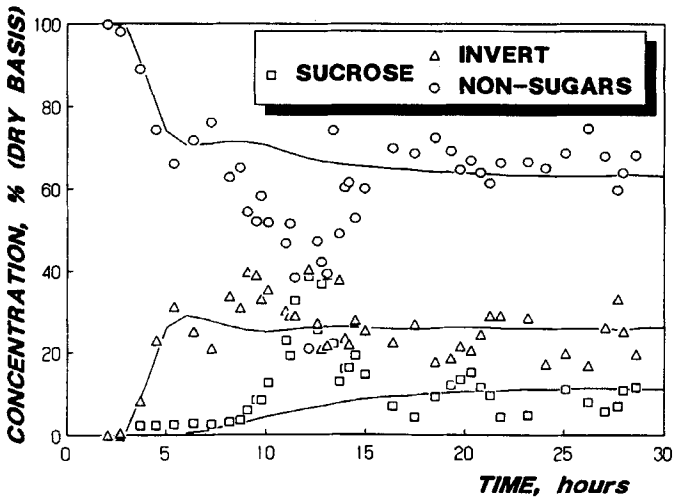

FIG. 13. Experimental (points) and simulated (lines) composition of the raffinate. Same parameters as in Fig. 12.

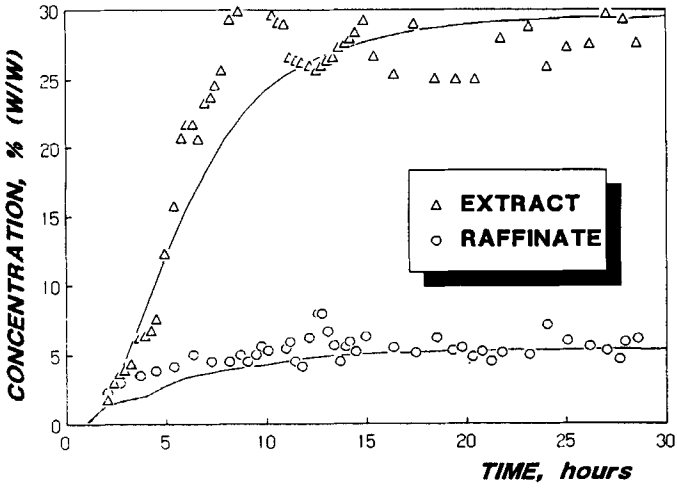

FIG. 14. Overall product concentrations. Experimental (points) and simulation (lines). Same parameters as in Fig. 12.

TABLE 3
Compositions of the Feed and Products, Average of Two 30-h Experiments, Feed Concentration 40.5%. All in Percent or ppm Dry Basis. Sucrose, Invert, and Nonsugars Determined by HPLC, the Rest by Atomic Absorption Spectrophotometry.

	Sucrose	Invert	Nonsugars	K^+	Na^+	P	Ca^{2+}	Mg^{2+}	Fe^{3+} ppm	Cu^{2+} ppm
Cane molasses	43.7	13.2	43.1	5.5	0.18	0.10	0.54	0.33	250	13
Treated molasses	—	—	—	5.5	2.0	0.27	0.11	0.18	66	16
Extract	79.2	12.8	8.0	1.1	0.15	0.04	0.00	0.00	83	23
Raffinate	10.1	18.5	71.4	8.8	2.0	0.45	0.06	0.01	541	91

hand, if extract is to be crystallized to produce solid sucrose, recirculation of invert into sucrose crystallization would be undesirable.

The fluid velocities (v) within the zones ranged from 24 to 34 cm/min (Fig. 12), the range of our pulse tests on the in-series columns. At 70°C, the temperature at which the simulated adsorber columns were kept, the HETP of sucrose is 5 cm in zone 1 and the recycle zone, and about 7 cm in zones II, III, and IV, so that each column corresponds to 42 and 30 theoretical stages, respectively. The dispersion comes primarily from mass transfer within the resin because of its small mean pore size, 10 Å, relative to the size of the sucrose molecule, ~5 to 7 Å.

Although the nonlinear and coupled isotherms found for pure components from pulse testing (Table 1) can be accommodated through an internal iteration within the SMB model, linear isotherms were found adequate to represent the dynamic behavior of the continuous adsorber, with the nonsugar component of molasses represented by equal fractions of a totally excluded species ($K = 0.00$) and a more retained fraction ($K = 0.25$), and 0.33 and 0.48 for sucrose and invert components, respectively. The agreement is excellent with the exception of the period at around 12 hours when problems with the system disrupted the steady operation. The semiempirical use of linear isotherms in modeling the simulated moving-bed adsorber, in particular the way of approximating the nonsugar behavior as a combination of an inert component and a linearly adsorbing species, may restrict the use of the model to applications with feeds of similar composition and concentration. It should still prove of value, though, in optimizing the separation, for a given feed, in respect to sizing the columns, flow rates within the zones and ports, and switch time. Further refinement of the model to include the nonlinear behavior will be done when more extensive experimental data from our continuous adsorber become available.

NOMENCLATURE

a	specific surface area of the resin ($= 6/d_p$), (cm^2/mL resin)
A	column cross-sectional area (cm^2)
A_i, B_i, K_{0i}	parameters of the adsorption isotherm of component i
c	liquid concentration (g/100 mL)
d_p	mean diameter of the resin particles (cm)
D_L	dispersion coefficient (cm^2/min)
F	flow rate (mL/min)
HETP	height equivalent to a theoretical plate (cm)
$HETP_{axial}$	contribution of the axial dispersion to HETP (cm)
$HETP_{film}$	contribution of the film mass transfer to HETP (cm)
$HETP_{intra}$	contribution of the intraparticle diffusion to HETP (cm)
k	overall mass transfer coefficient (L/min)
k_f	film mass transfer coefficient (cm/min)
K_i	partition coefficient of component i
L	column length (cm)
L'	effective bed length [$= L - \frac{1}{2}m_f/(\rho\epsilon A)$], (cm)
m_f	mass of feed (g)
q	solid concentration (g/100 mL solid phase)
t'	retention time of a component (see text), (min)
v	interstitial liquid velocity [$= F/(\epsilon A)$], (cm/min)
V'	retention volume of a component ($= Ft'/AL'$), (—)
ρ	liquid density (g/cm^3)
ϵ	bed porosity (—)

Acknowledgments

This research was supported by Grant LEQSF (1990-93)-RD-B-02 from the Louisiana Board of Regents. Donation of the resin by the Dow Chemical Company and financial support from the American Sugarcane League are gratefully acknowledged.

REFERENCES

1. P. C. Wankat, *Large-Scale Adsorption and Chromatography*, Vol. II, CRC Press, Boca Raton, Florida, 1986.
2. K. P. Chertudi, *Int. Sugar J., 28,* 93 (1991).
3. I. Kakihana, *Proc. Soc. Jpn. Sugar Ref. Tech., 11* (1989).
4. K. W. R. Schoenrock, 25th General Meeting of ASSBT, New Orleans, LA.
5. M. Saska, S. J. Clarke, M. D. Wu, and K. Iqbal, *J. Chromatogr., 590,* 147 (1992).
6. M. Mrini, M.S. Thesis, Lousisiana State University, Baton Rouge, Louisiana, 1991.
7. C. B. Ching, K. H. Chu, and D. M. Ruthven, *AIChE J., 36,* 275 (1990).
8. C. B. Ching, C. Ho, K. Hidajat, and D. M. Ruthven, *Chem. Eng. Sci., 42,* 2547 (1987).
9. U. P. Ernst and J. T. Hsu, *Ind. Eng. Chem. Res., 28,* 1211 (1989).
10. K. Hashimoto, M. Yamada, Y. Shirai, and S. Adachi, *J. Chem. Eng. Jpn., 20,* 405 (1987).

11. R. C. Weast (ed.), *Handbook of Chemistry and Physics,* 53rd ed., CRC Press, Cleveland, Ohio, 1973.
12. B. Lin and G. Guiochon, *Sep. Sci. Technol., 24,* 31 (1989).
13. W. Meyer, R. S. Olsen, and S. L. Kalwani, *Ind. Eng. Chem., Process. Des. Dev., 6,* 55 (1967).
14. C. B. Ching and D. M. Ruthven, *Chem. Eng. Sci., 40,* 877 (1985).
15. M. Goto, N. Hayashi, and S. Goto, *Sep. Sci. Technol., 18,* 475 (1983).
16. N. Wakao, T. Oshima, and S. Yagi, *Kagaku Kogaku, 22,* 780 (1958).

Received by editor January 27, 1992